Investigation of collective electron dynamics in relativistically transparent laser plasma interactions

Contact:ross.gray@strath.ac.uk ross.gray@strath.ac.uk

R.J Gray, D.A MacLellan, B. Gonzalez-Izquierdo, H.W Powell, R. Wilson and P. McKenna
SUPA Department of Physics, University of Strathclyde, Glasgow G4 0NG, UK

L.C Stockhausen and R. Torres
Centro de Láseres Pulsados (CLPU), M5 Parque Científico, 37185 Salamanca, Spain

M. Borghesi
Centre for Plasma Physics, Queens University Belfast, Belfast BT7 1NN, UK

D.C Carroll, G.G Scott, D.R Rusby, N. Booth, D.R Symes, S.J Hawkes and D. Neely
Central Laser Facility, STFC Rutherford Appleton Laboratory, Oxfordshire OX11 0QX, UK

C.D Murphy
SUPA School of Physics and Astronomy, University of Edinburgh, Edinburgh EH9 3JZ, UK

Abstract

The collective behaviour of pondermotively-driven electrons in the interaction of an ultraintense laser pulse with a relativistically transparent target is investigated both numerically and experimentally. The 2D profile of the electrons is found to lengthen along the laser polarisation axis in the case of limited transparency. At higher degrees of transparency a double lobe structure forms in the electron beam in the orthorgonal plane to the polarisation direction. Numerical results demonstrate good agreement with the experimentally measured degree of transparency and elucidate the laser-electron dynamics of the transition to transparency.

1 Introduction

Understanding the collective response of charged particles to intense laser radiation is not only of fundamental interest, but is also important for the development of potentially compact laser-driven electron [1] and ion [2, 3] accelerators. It also underpins a range of other intense laser-plasma physics, including high energy X-ray generation (bremsstrahlung [4], synchrotron [5, 6] and betatron [7] production), high harmonic generation [8], high-field physics [9], and the production of intense magnetic fields [10]. The collective expulsion of electrons from regions of higher to lower field amplitude occurs due to the ponderomotive force, which arises from the inhomogeneity of the oscillating electromagnetic fields [11]. For a linearly polarised laser pulse with electric field amplitude $\mathbf{E} = E(z)sin(\omega t)\hat{\mathbf{x}}$, travelling in the +z direction, the force exerted can be expressed as [12]:

$$\mathbf{f_p} = -\frac{e^2}{4\gamma m_e \omega^2}\frac{\partial}{\partial z}[E^2(z)[1 - cos(2\omega t)]]\hat{\mathbf{z}} \qquad (1)$$

where ω is the laser frequency, m_e is the electron mass and γ is the electron Lorentz factor. The first term is time-averaged and the second is a time-dependent component which drives longitudinal electron oscillations at twice the laser frequency (2ω) [12]. In a foil target, electrons are driven forward from the region of the critical density, n_c (beyond which the laser light cannot propagate), by the first component, with a 2ω oscillation induced by the second [12]. In the specific case of targets in which relativistic induced transparency (RIT) [13, 14, 15] occurs, the transmitted part of the laser pulse also ponderomotively drives a significant electron momentum in the perpendicular (radial) direction. RIT occurs in ultra-thin foils due to a combination of thermal expansion of the local target electron population and an increase in the critical density to γn_c due to the relativistic correction to m_e with increasing laser intensity. It can also occur if the laser longitudinal ponderomotive force decreases the target thickness to the order of the plasma skin depth [16, 17]. The former process is illustrated schematically in figure 1, which also shows the longitudinal propagation of a ponderomotively-driven local region of enhanced electron density ahead of the laser pulse [18]. Transparency changes the nature of the interaction from *surface-dominated* to *volumetric* [19], such that the collective electron response to the laser field continues over an extended distance. Understanding charged particle dynamics in the RIT regime is particularly important for the development of promising new ion acceleration mechanisms such as Break-Out Afterburner (BOA) [20, 21] and RIT-Acceleration (RITA) [18], and for schemes for which it is detrimental, such as radiation pressure acceleration (RPA) [22, 23, 24] (which is most effective just before transparency occurs).

In this report, we relate an experimental demonstration of an asymmetry in the collective electron response to the radial ponderomotive force during RIT, as manifested in the formation of elipsoidal and lobed structures in the spatial-intensity profile of the beam of accelerated electrons. In addition the electron dynamics during the

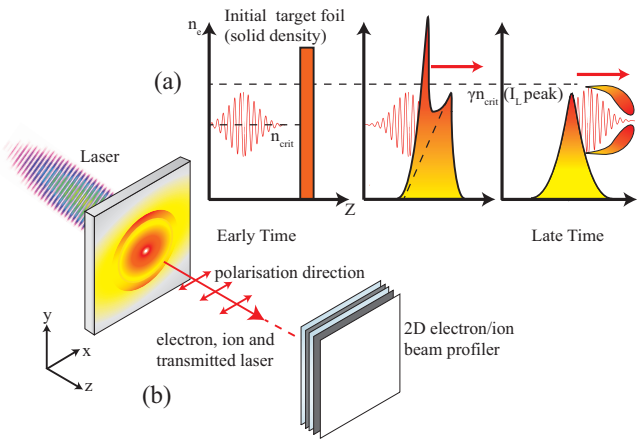

Figure 1: (a) Schematic illustrating the target electron density evolution and induced transparency. See main text for description. (b) Schematic showing the laser foil interaction and the position of the electron and proton spatial-intensity distribution detector.

onset of RIT are explored using numerical simulations.

2 Experiment

The Astra-Gemini Ti:sapphire laser at the Rutherford Appleton Laboratory was used to produce pulses of 800 nm wavelength, λ, light, with typical duration, τ =40 fs (full width at half maximum, FWHM), spot size of 3 μm (FWHM) and energy $\sim$2 J (on-target, i.e. the energy after plasma mirrors and transport optics). A double plasma mirror arrangement enhanced the intensity contrast to $\sim 10^{11}$ and $\sim 10^{9}$, at 1 ns and 10 ps, respectively, prior to the peak of the pulse. The pulse was focused using an f/2 parabolic mirror, to a calculated peak intensity, I, of 7×10^{20} Wcm^{-2} and incident along the target normal axis. A deformable mirror was employed prior to focusing to ensure a high quality focal spot. The laser light was linearly polarised, with the direction of polarisation varied using a thin mica $\lambda/2$ wave-plate. The target was an aluminium foil, with thickness, L, varied in the range $10 - 800$ nm. The energy of the portion of the laser light transmitted through the target (due to RIT) was monitored both by optical spectrometer measurements and by measuring the 2D spatial-intensity profile of the transmitted laser beam on a PTFE screen positioned behind the target, with a CCD camera. The energy transmission as measured by both diagnostics was calibrated by comparing the recorded signal to the energy measured on a calorimeter on shots for which there was no target in the beam path.

The 2D spatial-intensity profile of the beam of electrons ponderomotively accelerated by the laser pulse was measured 3 cm downstream from the target using passive stacked layers of Fujifilm imaging plate (IP), interleaved with iron filters.

Figure 2 shows representative measurements of the spatial-intensity profile of the electron beam, and exhibits the most salient features of the experimental results. The only laser pulse parameter varied for this data set is the direction of polarisation (τ=40 fs and I=7 $\times$ 10^{20} Wcm^{-2}). For L = 800 nm, for which induced transparency does not occur, the electron beam is circular and relatively small. For L = 40 nm, a larger number of electrons are detected and the beam is highly elliptical, with the major axis parallel to the laser polarisation. This is clear when comparing figure 2(b) and (c), for which the laser polarisation vector is along the x- and y-axis, respectively. Similar polarisation-sensitive electron beam ellipticity has been previously observed in laser-underdense plasma interactions [26] (but not with overdense targets) and indicates strong electron interaction with the laser electric field.

Figure 2(d) shows the corresponding case for polarisation in x and a L = 10 nm target, for which a double-lobe structure, centred on the laser propagation axis and orientated in the axis perpendicular to the laser polarisation, is measured. A more detailed discussion of the mechanism which drives the double-lobe structure is beyond the scope of this report but is the subject of another publication by the authors [27].

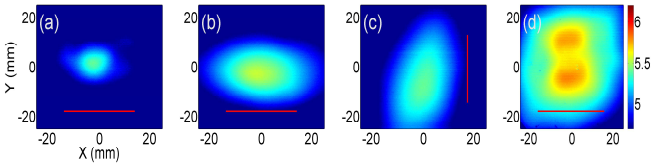

Figure 2: (a)-(d) 2D spatial-intensity distribution of the electron beam, for energy > 5 MeV, as measured with imaging plate, for: (a) L =800 nm with polarisation in the x-axis; (b) L =40 nm with polarisation in the x-axis; (c) L =40 nm with polarisation in the y-axis; and, (d) L =10 nm with polarisation in the x-axis. The laser polarisation axis is shown as a red line.

3 Simulations

To investigate the onset of RIT in more detail, 2D3V simulations were performed using the fully relativistic electromagnetic PIC code EPOCH. The simulation grid comprised a total of 7.2 million cells with up to 960 particles per cell and a spatial resolution of 0.5 $\times$ 0.8 nm. The laser pulse had a Gaussian profile both temporally and spatially. The target consisted of two species, electrons and Al^{13+} ions at a density $n_e/n_{cr} = 447$. In order to resolve the Debye length the initial electron and ion temperatures were $T_e = 10$ keV and $T_i = 40$ eV, respectively. Simulations were performed as a function of laser polarisation, target thickness (10, 20 and 40 nm) and laser intensity (up to 7$\times$10^{20} Wcm^{-2}). The simulation

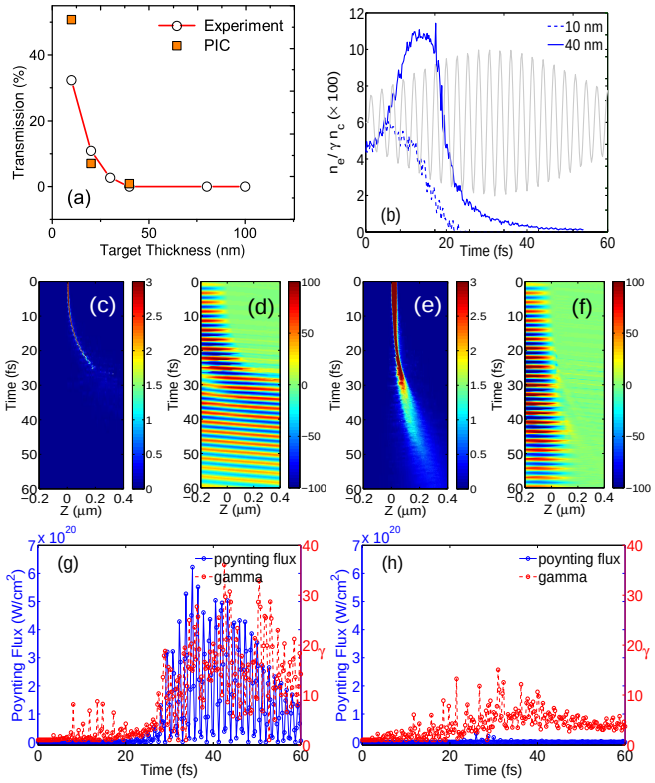

Figure 3: (a) Comparison between experiment and simulation results for the transmitted percentage of the laser pulse energy as a function of target thickness. (b) Evolution of the peak electron density in the PIC simulation (at any position across the evolving electron density profile) for L=10 nm and 40 nm. The laser pulse temporal profile is shown in the background for reference. (c) Electron density (in units of $100n_e/n_c$) and (d) laser electric field (in units of TV/m) along the laser propagation (z) axis as a function of time, for L=10 nm; (e) and (f) are the corresponding plots (same units) for L=40 nm; (g) Evolution of the laser Poynting flux and the electron Lorentz factor 600 nm from the target rear surface for L=10 nm; (h) Corresponding plots for L=40 nm.

plane is y-z and the laser is incident along target normal (z-axis) and propagates only 200 nm in vacuum before reaching the target front surface (laser light therefore reaches the target 1.5 fs after the start of the simulation, ensuring interaction with an initially solid density target).

As shown in figure 3(a), the predicted onset of transparency is in good agreement with the experimental results, albeit that the percentage of transmitted light is higher than that measured for the 10 nm-thick target case. Simulations for L =40 nm exhibit minimal transparency. As shown in figure 3(b), for this case the peak electron density increases by more than a factor 2 in response to the laser ponderomotive drive, and decreases to γn_c only very late in the laser pulse cycle (which is included as a background plot). By contrast, for L =10 nm significant transparency occurs as the peak density decreases to γn_c on the rising edge of the laser pulse. The temporal evolution of the electron density and the laser electric field along the laser propagation axis (y=0) is shown in figure 3(c) and (d), respectively, for L =10 nm, and in figure 3(e) and (f), respectively, for L =40 nm. The effects of radiation pressure are observed in both cases, with the L=10 nm target becoming transparent after 30 fs. The L=40 nm case remains overdense throughout the simulation time.

The evolution of the electron Lorentz factor and the Poynting flux, which is a diagnostic of laser energy, at an example distance of 600 nm downstream from the initial rear surface of the target, are shown in figure 3(g) and (h), for L =10 nm and 40 nm, respectively. For the L =10 nm case transparency occurs after ∼30 fs, and the Lorentz factor increases by more than a factor of two in response to the transmitted laser pulse. There is no appreciable increase in the electron Lorentz factor downstream for the L =40 nm case. The results presented in figure 3 all involve polarisation in the plane of the simulation box. These results confirm that for the parameters of the experiment, significant transparency occurs for L =10 nm and that the propagated portion of the laser pulse continues to act on the accelerated electrons over an extended volume at the target rear.

4 Summary

In summary, the collective dynamics of electrons in a relativistically transparent foil driven by a linearly polarised laser field is experimentally shown to exhibit an ellipsoidal structure in the case of limited transparency and a double lobe structure for large degrees of transparency in the electron density distribution. Furthermore numerical simulations of the onset of RIT demonstrate a strong additional heating of accelerated electrons as the laser pulse is transmitted through the target, resulting in a transition from a *surface* to a *volume* absorption regime.

5 Acknowledgements

We acknowledge the expert support of the staff at the Central Laser Facility of the Rutherford Appleton Laboratory and the use of the ARCHIE-WeST high performance computer. This work is supported by EPSRC (grant numbers EP/J003832/1, EP/L001357/1 and EP/K022415/1), LASERLAB-EUROPE (grant agreement n 284464, EC's Seventh Framework Programme) and sponsored by the Air Force Office of Scientific Research, Air Force Material Command, USAF (grant number FA8655-13-1-3008). LCS acknowledges LA^{3}NET, which is funded by the European Commission under Grant Agreement Number GA-ITN-2011-289191. The EPOCH code was developed under EPSRC grant EP/G054940/1.

References

[1] E. Esarey, C.B. Schroeder, W. P. Leemans, Rev. Mod. Phys., **81**, 1229 (2009)

[2] H. Daido, M. Nishiuchi and A.S. Pirozhkov, Rep. Prog. Phys., **75**, 056401 (2012)

[3] A. Macchi, M. Borghesi and M. Passoni, Rev. Mod. Phys., **85**, 751 (2013)

[4] P.A. Norreys *et al.*, et al., Phys. Plasmas **6**, 215 (1999)

[5] S. Kneip *et al.*, Nat. Phys. **6**, 980 (2010)

[6] A. Rousse *et al.*, Phys. Rev. Lett. **93**, 135005 (2004)

[7] S. Cipiccia *et al.*, Nat. Phys. **7**, 867 (2011)

[8] B. Dromey *et al.*, Nat. Phys. **8**, 804 (2012)

[9] A.R. Bell and J.G. Kirk, Phys. Rev. Lett. **101**, 200403 (2008)

[10] A.R. Bell and R.J. Kingham, Phys. Rev. Lett. **91**, 035003 (2003)

[11] T.W.B. Kibble, Phys. Rev. Lett., **16**, 1054 (1966)

[12] W.L Kruer and K. Estabrook, Phys. Fluids, **16**, 430 (1985)

[13] P. Kaw and J. Dawson, Phys. Fluids **13**, 472 (1970)

[14] A.I. Akhiezer and R.V. Polovin, Soviet Phys. JETP, **3** (1956)

[15] S. Guerin *et al.*, Phys. Plasmas, **3**, 2693 (1996)

[16] V.A. Vshivkov *et al.*, Phys. Plasmas, **5**, 2727 (1998)

[17] W. Yu *et al.*, Phys. Rev. E, **59**, 3583 (1999)

[18] A.A. Sahai *et al.*, Phys. Rev. E., **88**, 043105 (2013)

[19] A. Henig *et al.*, Phys. Rev. Lett. **103**, 045002 (2009)

[20] L. Yin *et al.*, Phys. Rev. Lett. **107**, 045003 (2011)

[21] D. Jung *et al.*, New J. Phys. **15**, 123035 (2013)

[22] T. Esirkepov *et al.*, Phys. Rev. Lett. **92**, 175003 (2004)

[23] A. Henig *et al.*, Phys. Rev. Lett. **103**, 245003 (2009)

[24] S. Kar *et al.*, Phys. Rev. Lett. **109**, 185006 (2012)

[25] B.M. Hegelich *et al.*, New J. Phys., **15**, 085015 (2013)

[26] S.P.D. Mangles *et al.*, Phys. Rev. Lett, **96**, 215001 (2006)

[27] R.J Gray *et al.* , currently under review. (2014)